

Accelerating Gaussian beam tracing method with dynamic parallelism on graphics processing units

Zhang Sheng^{a,c}, Lishu Duan^{a,d,*}, Hanbo Jiang^{a,b,**}

^a*Eastern Institute for Advanced Study, Eastern Institute of Technology, Ningbo, China*

^b*Ningbo Institute of Digital Twin, Eastern Institute of Technology, Ningbo, China*

^c*School of Mathematics, Hefei University of Technology, Hefei, China*

^d*School of Ocean and Civil Engineering, Shanghai Jiao Tong University, Shanghai, China*

Abstract

This study presents a reconstruction of the Gaussian Beam Tracing solution using CUDA, with a particular focus on the utilisation of GPU acceleration as a means of overcoming the performance limitations of traditional CPU algorithms in complex acoustic simulations. The algorithm is implemented and optimised on the NVIDIA RTX A6000 GPU, resulting in a notable enhancement in the performance of the Gaussian Beam Summation (GBS) process. In particular, the GPU-accelerated GBS algorithm demonstrated a significant enhancement in performance, reaching up to 790 times faster in city environment and 188 times faster in open plane environment compared to the original CPU-based program. To address the challenges of acceleration, the study introduces innovative solutions for handling irregular loops and GPU memory limitations, ensuring the efficient processing of large quantities of rays beyond the GPU's single-process capacity. Furthermore, this work established performance evaluation strategies crucial for analysing and reconstructing similar algorithms. Additionally, the study explored future directions for further accelerating the algorithm, laying the groundwork for ongoing improvements.

Keywords: Beam tracing, GPU acceleration, dynamic parallelism

*Corresponding author. Email: duanlishu@sjtu.edu.cn

**Corresponding author. Email: hjiang@eitech.edu.cn

1. Introduction

The study of sound propagation is crucial for a wide range of applications, including the design of concert halls [1, 2], the enhancement of virtual reality experiences [3], improvements in audio prediction for gaming [4, 5], and the assessment of environmental noise from drones and unmanned aerial vehicles [6, 7, 8]. One of the key challenges in acoustics simulation is modeling the interaction of sound waves with complex environments, which involves reflections, diffractions, and scattering.

Over the past few decades, various simulation approaches have been developed to address these challenges, broadly classified into wave-based and geometrical acoustics [9, 10, 11]. Wave-based methods directly solve the wave equation to capture phenomena like interference and diffraction, while the traditional numerical method such as finite element method [9] and finite difference method [12] are adopted. Despite these methods provide good accuracy, their substantial computational demands make them inappropriate for large-scale applications with complex geometries. Conversely, geometrical acoustics simplifies sound as rays or beams and models reflections in a computationally efficient manner, making it particularly useful for large environments [13]. In this regard, the image source method and ray tracing method are widely used in various acoustic applications. The image source method [14] models each reflection from a surface as if it originates from an image source symmetrically positioned on the opposite side of that surface. This method is highly effective for simpler environment such as predicting room impulse responses, analyzing reverberation, and optimizing sound design in spaces like auditoriums and studios. However, as the order of reflections increases, particularly in environments with dense occlusions, the number of image sources grows exponentially, leading to a significant increase in computational complexity [13].

On the other hand, the ray tracing method represents sound as a collection of rays that emanate from a source [15]. These rays travel through the environment and interact with surfaces encountered. Various versions of the ray tracing algorithm have been implemented ever since the pioneering work of Krokstadt et al. [16]. However, the standard ray tracing method suffers perfect shadows and caustics [17]. To address these limitations, the Gaussian beam tracing (GBT) method was introduced as an extension to traditional ray tracing method [17]. This approach associates each ray with a beam that has a Gaussian intensity distribution then constructs the sound

at any given point by summing the contributions of each beam [18]. Unlike traditional rays, Gaussian beams inherently spread sound energy over a continuous area, filling in gaps where traditional rays might fail. The improvements are twofold: Physically, Gaussian beams allow for smooth transitions in sound intensity across space, preventing infinite energy accumulation in caustic regions and reducing unwanted spikes or dips in sound pressure [17]. Numerically, Gaussian beams enhance sound field coverage while requiring fewer computational resources. This proves particularly advantageous in complex environments with numerous reflections and refractions [6], as it reduces artifacts that would otherwise demand significant post-processing.

Nevertheless, GBT method still faces challenges, particularly in large environments with complex geometries, where the number of beams and interactions increases significantly, leading to higher computational demands. To address these limitations, parallel computation can be employed. It distributes computational tasks across multiple processing units, thereby reducing the time required to trace beams, compute interactions, and reconstruct the sound field. Among parallel architectures, graphics processing units (GPUs) have proven particularly effective due to their ability to handle many tasks simultaneously. GPUs are equipped with thousands of cores that can process numerous parallel tasks concurrently, making them well-suited for data-intensive applications and independent tasks [19]. This architecture provides significant speedups for highly parallel tasks [20], such as those encountered in geometric acoustics. Spjut et al. investigated a multi-threaded beam tracing algorithm on multicore platforms, achieving significant speedups with an increased number of threads [21]. Cowan and Kapralos discussed GPU ray tracing techniques and demonstrated performance improvements for real-time acoustic prediction [22]. Gkanos et al. implemented the image source method on multiple GPUs and suggested that incorporating beam tracing could further enhance efficiency [23]. Tan et al. proposed a GPU-based tree-accelerated beam-tracing method, achieving a speedup of 66 times compared to conventional techniques [24]. Additionally, Greef et al. employed a ray tracing algorithm for radiotherapy dose calculations on a GPU, achieving a 6 times speedup for the evaluated cases [25].

While significant advancements have been made in accelerating Ray Tracing(RT) method, which is only a part of GBT, the reconstruction of the sound pressure field remains underexplored. This crucial process involves searching for all beams contributing to the sound pressure at a specific field point. Existing approaches do not fully leverage parallel computation capabilities,

leading to inefficiencies. This study proposes the use of dynamic parallelism on GPUs, which allows for on-the-fly parallel task generation [26]. By enabling kernels to launch other kernels, this method allows threads to manage their parallelism dynamically without the need for explicit synchronization through the host. This approach not only reduces the overhead of kernel launches but also improves overall resource utilization, which is particularly beneficial for collecting contributions from all Gaussian beams where the computational load varies from point to point [27, 28].

The remainder of this paper is organized as follows: Section 2 introduces the fundamental principles of Gaussian Beam Tracing (GBT), including its mathematical framework and the computational challenges encountered in large-scale acoustic simulations. Section 3 details the development of the GPU-accelerated algorithm, emphasizing the integration of flat and dynamic parallelism to address bottlenecks in computational performance. The implementation strategies, including memory management and workload balancing, are also discussed. Section 4 presents the validation of the proposed method against analytical solutions, followed by a comprehensive performance evaluation in different acoustic environments. Section 5 explores numerical experiments conducted in both free-field and city environments, highlighting the significant performance gains achieved with the optimized GPU algorithm and identifying the remaining limitations. Finally, Section 6 concludes the paper by summarizing the key findings and proposing future directions for further research and optimization.

2. Gaussian beam tracing

Figure 1 illustrates the Gaussian beam model, where the ray represents the path of sound propagation and is typically computed using a ray tracing algorithm. The Gaussian-shaped energy distribution around the ray is given by the following expression:

$$p(s, q_1, q_2, t) = \phi \left(\frac{C(s)}{\det[Q(s)]} \right)^{1/2} \times \exp \left[-i\omega \left(t - \int_s^{s_0} \frac{ds}{C(s)} \right) + \frac{i\omega}{2} (\mathbf{q}^T P Q^{-1} \mathbf{q}) \right], \quad (1)$$

where ϕ is a real constant, and (s, q_1, q_2) represent the ray-centered coordinates. Here, $\det[\cdot]$ represents the determinant operator, and P and Q are

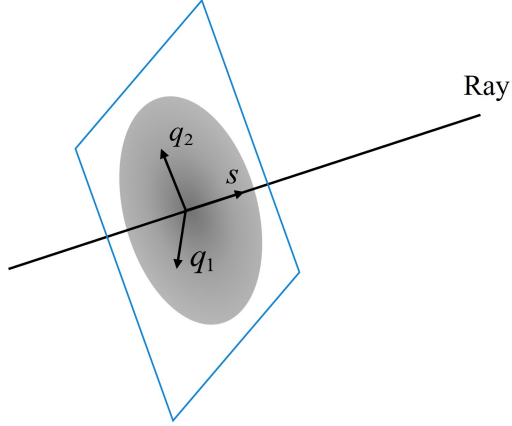


Figure 1: Schematic of a Gaussian beam and the associated coordinates.

matrices that satisfy the following relations:

$$\frac{\partial Q}{\partial s} = cP, \quad \frac{\partial P}{\partial s} = 0, \quad (2)$$

where c is the sound speed. The method for calculating ray paths has been extensively studied and will therefore not be repeated here. Interested readers are encouraged to refer to the relevant literature for more detailed implementations [29]. Subsequently, the contributions of all nearby Gaussian beams along each ray are gathered to estimate the sound pressure p at any observation point R

$$p(R, \omega) = \int \int \Phi(\gamma_1, \gamma_2) P(R_\gamma, \omega) \exp[i\omega T(R, R_\gamma)] d\gamma_1 d\gamma_2, \quad (3)$$

where $\Phi(\gamma_1, \gamma_2)$ is the weighting function, $P(R_\gamma, \omega)$ represents the complex amplitude along the ray R_γ , and $T(R, R_\gamma)$ is the propagation time from the point R_γ to R . In this formula, another important coordinates called ray coordinates (s, γ_1, γ_2) is presented, which are connected to the whole ray field, and γ_1 and γ_2 are the parameters of the ray at the source. For more details on the GBT method, please refer to the literature [6]. It is worth noting that numerically evaluating the above integration is time-consuming, but this process can be significantly accelerated using GPU calculations.

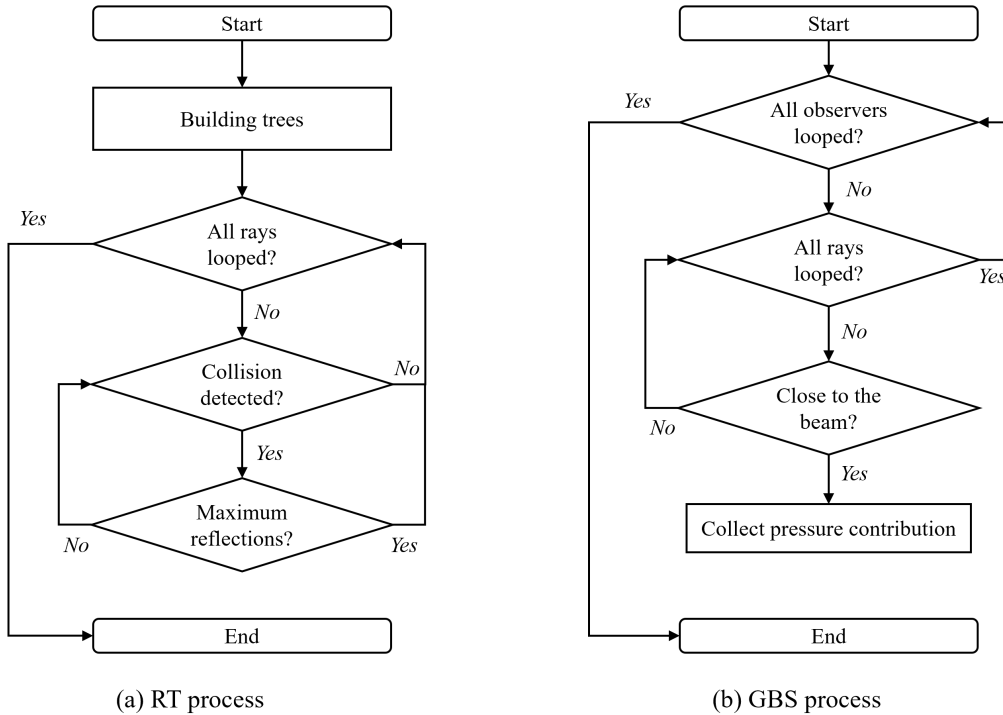


Figure 2: The programming flowcharts of the RT and GBS processes. The proposed dynamic parallelism targets to accelerate looping all rays in each process.

3. Algorithm and implementation

3.1. Overview

This section presents the numerical algorithm for Gaussian beam tracing and its parallel implementation. The overall workflow consists of two primary processes: ray tracing (RT) and Gaussian beam summation (GBS), as illustrated in Fig. 2. In the RT process, sound propagation paths are determined by tracing rays and modeling their interactions with obstacles. The complexity of this stage is driven by the number of rays and boundary elements, where the latter are typically triangular facets representing reflective surfaces. Subsequently, the GBS process aggregates contributions from all Gaussian beams to calculate sound pressure at observation points. Its computational demand is primarily influenced by the number of rays and observation points.

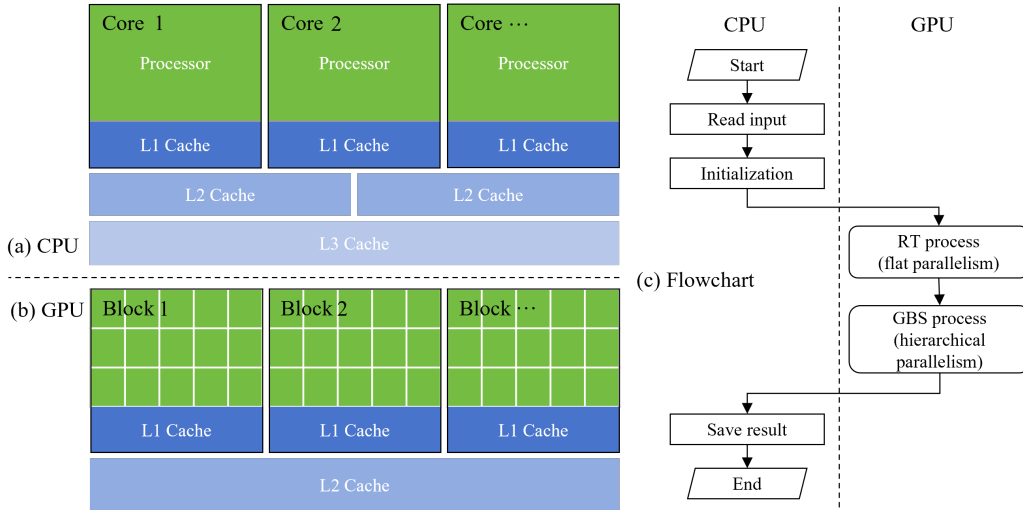


Figure 3: (a) Typical CPU architecture; (b) Typical GPU architecture; Green indicates the processor while blue represents the memory; (c) Flowchart of the GPU acceleration implementation.

3.2. CUDA architecture

We now turn to the numerical implementations utilizing the compute unified device architecture (CUDA), a parallel computing platform and application programming interface developed by NVIDIA[®]. The CUDA programming model enables us to leverage computational resources from both CPU and GPU platforms. Fig. 3(a) illustrates the memory hierarchy in CPUs, consisting of three levels of cache memory: L1, L2, and L3. L1 performs the smallest and fastest, directly integrated into each core; L2 denotes larger and slower, dedicated to each core or shared among a few cores; and L3 represents the largest and slowest, shared across all cores, acting as a buffer between the cores and the main memory (random access memory, RAM). In contrast, the GPU functions as a computation grid, consisting of hundreds of blocks, each containing thousands of processors, as shown in Fig. 3(b). Threads within these blocks run concurrently, processing data in parallel using shared L1 cache memory. Each block can execute cooperatively via barrier synchronization. However, blocks typically do not share data directly with one another, except through global memory (L2) or other memory structures.

The proposed GBT implementation consists of both sequential and parallel components. As shown in Fig. 3(c), tasks with low degrees of parallelism,

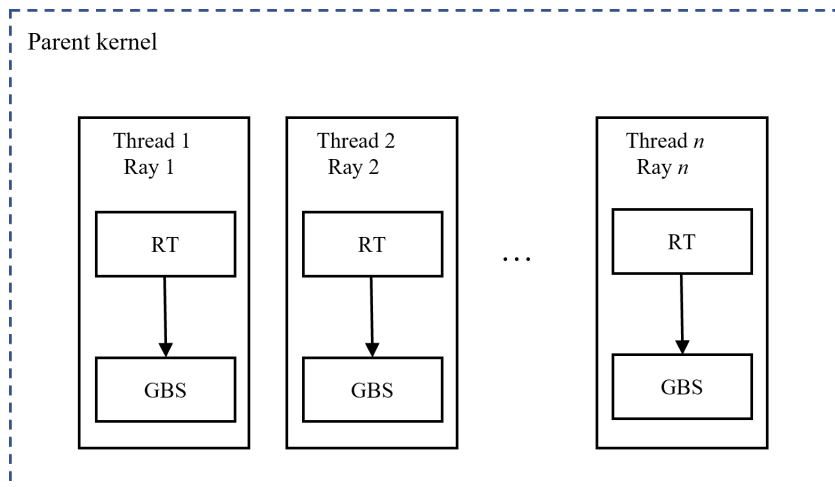


Figure 4: The multi-threaded programming model of flat parallelism on GPU. These threads run simultaneously.

such as file input/output operations, are assigned to the CPU to fully leverage its strengths and efficiency in sequential processing. Conversely, tasks like the RT and GBS processes, which involve high degrees of parallelism and heavy computational loads, are offloaded to the GPU which excels at handling numerous parallel operations simultaneously. Once these computations are completed, the results are transferred back to the CPU, where the remaining output and prediction processes continue in the same manner as the traditional CPU algorithm. This division of workflow ensures optimal utilization of each processor based on the nature of the tasks.

3.3. Flat parallelism

Figure. 4 illustrates the flowchart of flat parallelism, detailing the entire algorithmic process of executing the RT and GBS steps. The algorithm handles an array of rays, with the initial direction of each ray defined by specified combinations of elevation and azimuth angles. Each ray’s computation, encompassing both RT and GBS processes, is assigned to a dedicated thread. By evenly distributing these tasks across processors, flat parallelism fully exploits the computational capabilities of GPUs. After all rays are looped, the GPU computation finished and the whole workflow enters CPU phase.

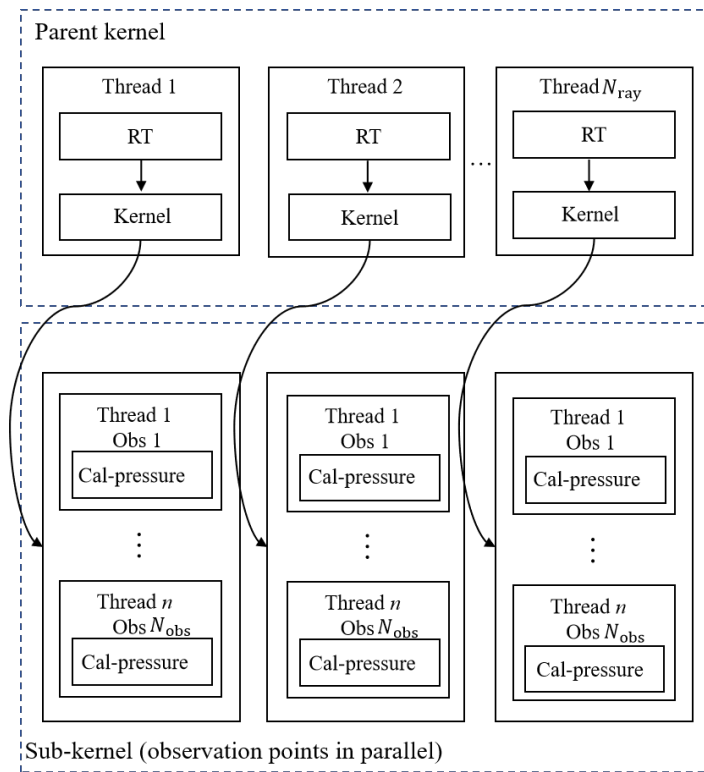


Figure 5: The multi-threaded programming model of dynamic parallelism on GPU.

3.4. *Dynamic parallelism*

In GBT process, each beam appears to be independent, making it well-suited for flat parallelism. However, the computational load varies across different observers and beams. This variation arises from the need to loop through all beams that contribute to the sound pressure in the GBS process, as described by Eq. (3). The length of each beam can vary significantly, especially in complex environments where sound propagation is more intricate. Using flat parallelism resulted in uneven execution times: lightly loaded threads completed quickly, leaving heavy tasks to dominate the overall runtime.

To address these inefficiencies, the present study adopts dynamic parallelism, a technology introduced by NVIDIA [26], which allows kernels to launch additional kernels during execution, as illustrated in Fig. 5. This hierarchical execution model enables fine-grained control over task allocation and workload balancing. Specifically, when a thread encounters a computationally intensive task, it can dynamically spawn child kernels to divide the workload further. These child kernels are executed independently, allowing idle GPU cores to be reallocated in real time to assist with heavy tasks. This mechanism ensures that computational resources are utilized efficiently, reducing idle time and mitigating bottlenecks.

Figure. 6 compares flat and dynamic parallelism. In flat parallelism, tasks are statically distributed across GPU threads during kernel launches. This approach often leads to inefficiencies, as lightly loaded threads finish early and remain idle, while heavily loaded threads create bottlenecks. In contrast, dynamic parallelism redistributes the workload dynamically, enabling idle cores to assist heavily loaded threads. This adaptive rebalancing accelerates task execution significantly reduces overall computation time. The transition from flat to dynamic parallelism is particularly advantageous in environments with highly non-uniform task distributions, ensuring better load balancing and more efficient resource utilization.

4. Results and discussion

4.1. *Verification*

To verify the correctness of the method described in this paper, the reflection of a monopole sound source above an infinitely long plate was computed. The results obtained by the GBT method are compared with the analytical solution. The sound source is positioned at $z = 5$ with a frequency of 500Hz.

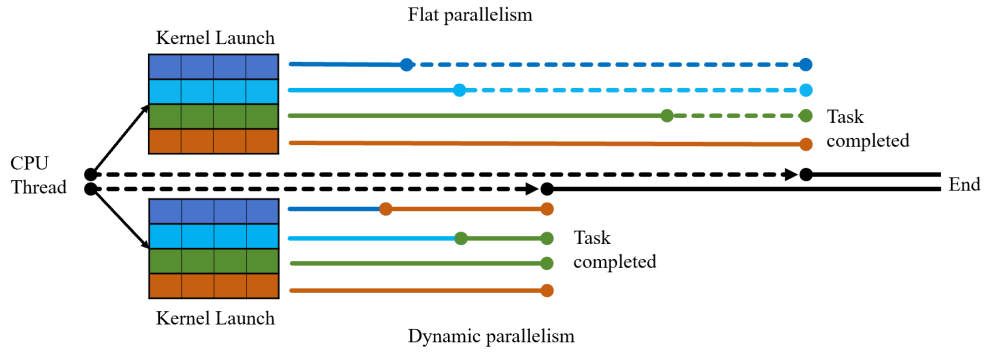


Figure 6: Comparison between flat and dynamic parallelisms.

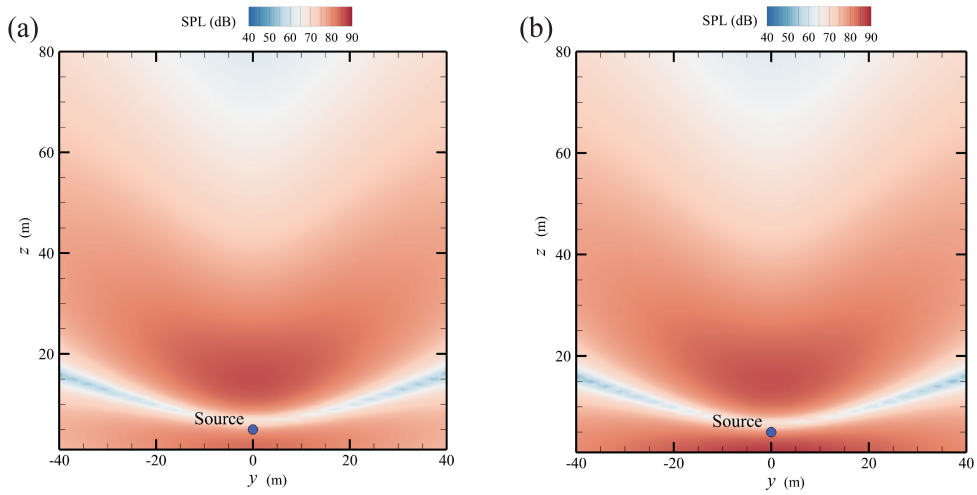


Figure 7: Comparison of whole SPL calculated by (a) GBT method and (b) analytical solution at $f = 50\text{Hz}$.

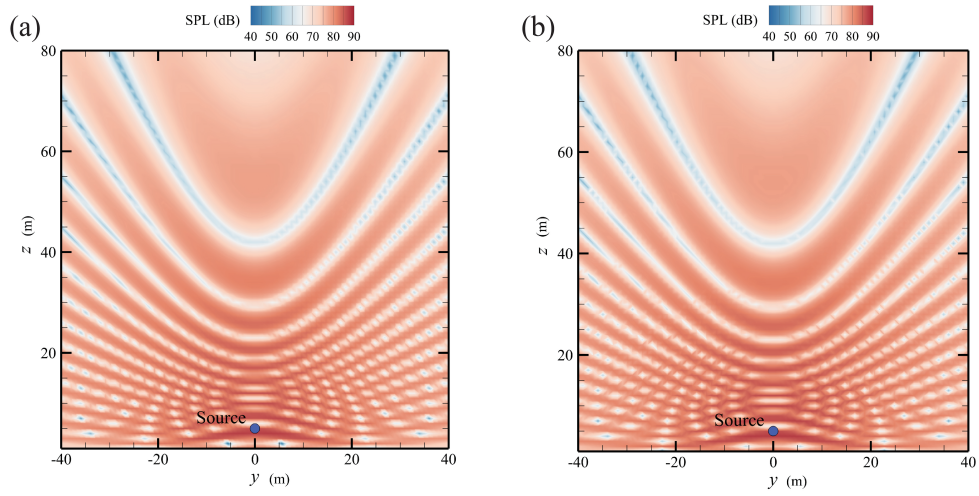


Figure 8: Comparison of whole SPL calculated by (a) GBT method and (b) analytical solution at $f = 500\text{Hz}$.

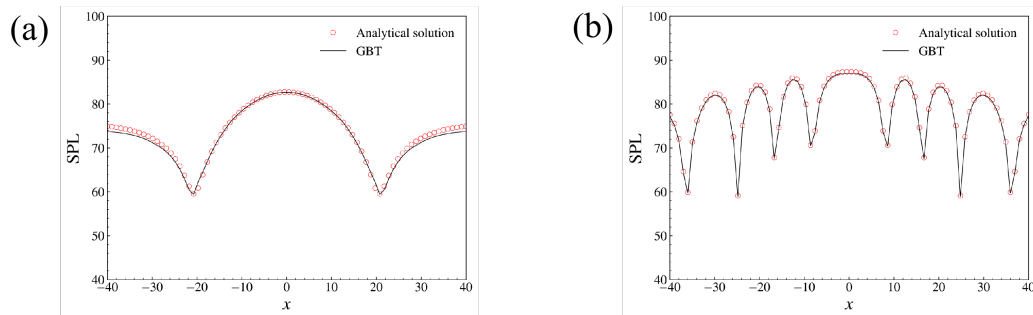


Figure 9: Comparison of SPL at $z = 10$ using dynamic range with error bars for various frequencies: (a) 50Hz, (b) 500Hz.

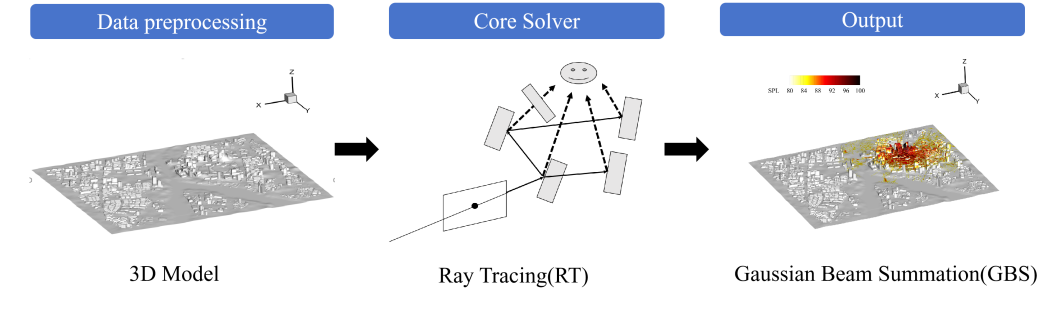


Figure 10: Single-threaded sound field prediction algorithm framework.

Figure. 7 compares the sound field of a monopole sound source positioned above a rigid ground at $z = 5\text{m}$ with a frequency of 50Hz . The results demonstrate that the GBT solver reliably reproduces the sound field structure, as validated against the analytical solution. Fig. 8 also illustrates the case for a sound source frequency of 500Hz , where the GBT solver’s results continue to closely match the analytical solution. The comparison further confirms the solver’s accuracy across different frequencies. Fig. 9 compares the sound pressure level distribution at $z = 10$, showing an excellent match between the two results.

This validation case demonstrates the accuracy of the proposed method and its implementation even for high-frequency sound reflection problems, providing a strong foundation for subsequent calculations.

4.2. Application to environmental noise

In the GBT algorithm, key information such as the characteristics of the noise source, the geometric environment model, and the observer’s position are taken as inputs, which then transforms the geometric objects in the inputs into structures optimized for accelerated processing. Subsequently, the RT module are responsible for executing two core tasks: calculating the propagation trajectories of each Gaussian beam and predicting the sound pressure contributions of these beams along their propagation paths. For each observation point, the final calculation of sound pressure is completed through the GBS module. This method involves integrating the contributions of all Gaussian beams near the observation point to construct the complete sound field. This entire computational process is detailed in Fig. 10.

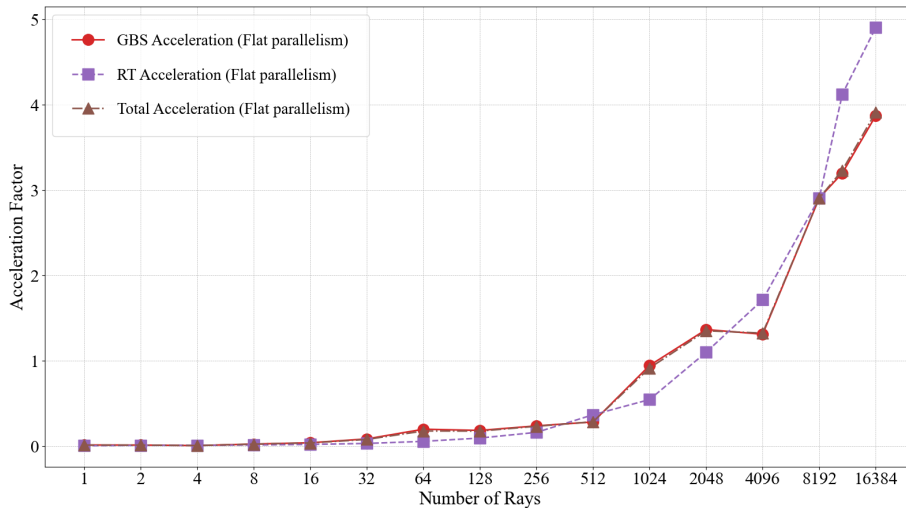


Figure 11: Performance comparison of multithreaded sound field prediction using flat parallelism GPUs: Acceleration factor for different ray counts.

4.3. Numerical tests for GPU acceleration without dynamic parallelism

In the preliminary phase of this study, the focus is on migrating existing single-threaded sound field prediction algorithms to the GPU platform, aiming to enhance computational efficiency through hardware acceleration. The experimental scenario involves complex city environments. Experimental results demonstrate that, compared to sequential execution on a CPU, the acceleration effect achieved by leveraging GPU capabilities is illustrated in fig. 11 and fig. 12. These figures likely showcase significant improvements in processing time and efficiency, highlighting the benefits of utilizing GPU acceleration for sound field prediction in complex environment.

In the experiments, we observed that as the number of rays increased, the acceleration factor for GBS gradually improved, starting from an initial factor of 0.013 and increasing up to 3.47. This indicates that GPU acceleration becomes increasingly efficient in processing GBS computations as the number of rays grows. Similarly, the acceleration factor for Ray Tracing (RT) also showed a certain growth trend, increasing from an initial factor of 0.04 up to 4.90.

With the increase in the number of rays, both the GBS and RT acceleration factors exhibited improvements. Given that the GBS part occupies more than 95% of the total computation time, the overall acceleration factor

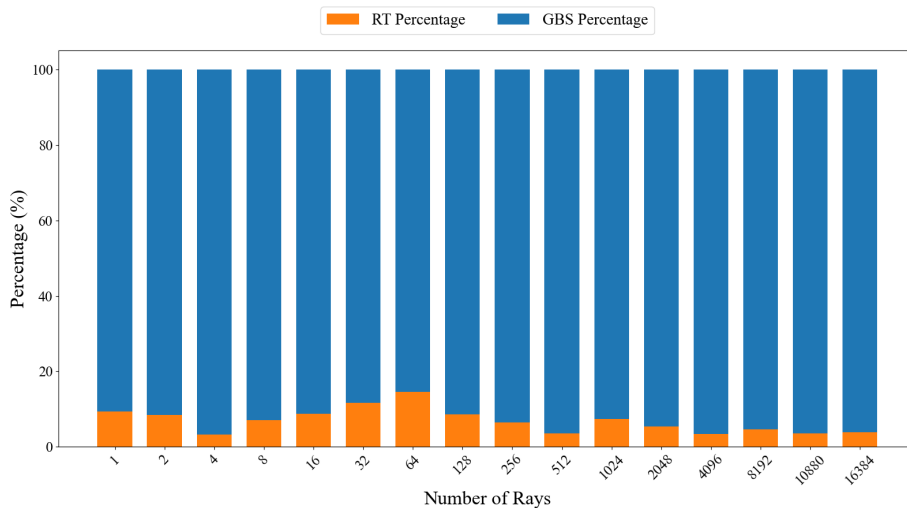


Figure 12: Percentage of two main processes in a multi-threaded sound field prediction algorithm using flat parallelism GPUs.

is close to that of GBS. These results indicate that despite the observed acceleration effect, the overall acceleration performance is still limited due to the influence of the number of rays on the number of parallel GPU threads and the fact that the single-thread performance of GPUs is much lower compared to CPUs.

To further analyze the GPU performance utilization, we employ NVIDIA’s performance analysis tool, Nsight Compute. This tool can provide detailed GPU performance metrics, helping us understand the efficiency of the program’s execution on the GPU. The analysis results are presented in Table 1.

Table 1: GPU Speed Of Light Throughput Metrics

Metric	Throughput [%]
Compute (SM) Throughput	3.23
Memory Throughput	1.68
L1/TEX Cache Throughput	24.64
L2 Cache Throughput	1.68
DRAM Throughput	0.50

The Compute (SM) Throughput of 3.23% represents the efficiency of the

Streaming Multiprocessors (SMs) on the GPU when executing computational tasks relative to their theoretical maximum efficiency. This low percentage indicates that the utilization of computational resources is not high, and improving their utilization is a top priority.

Although the use of the GPU platform has achieved computational acceleration to some extent, the efficiency gains are limited when dealing with complex acoustic environments and high-density ray grids. Especially in environment involving high-frequency sound waves and complex environmental interactions, relying solely on the hardware advantages of GPUs has not fully addressed the performance bottlenecks in sound field prediction, leading to significant limitations in computational efficiency.

4.4. Numerical test for GPU acceleration with dynamic parallelization

After implementing dynamic parallel optimization for the sound field prediction algorithm, we conducted a detailed evaluation of the algorithm’s acceleration performance, with a particular focus on the performance improvement in the GBS section after introducing dynamic parallel processing. To ensure the effectiveness of the proposed algorithm and the accuracy of the performance evaluation, the hardware configuration included an NVIDIA RTX A6000 GPU and the CUDA version used was 12.03. This setup aimed to provide an efficient, stable, and reproducible experimental platform for evaluating the proposed multi-threaded sound field prediction algorithm. With such a configuration, the experimental results can effectively reflect the algorithm’s performance and provide valuable references for subsequent research and applications.

To evaluate the performance of the proposed multi-threaded sound field prediction algorithm, the program was executed under two different complexity environment - “Free Field” and “city environment”. In the experiments, we compare the performance of executing the same tasks using a single-threaded CPU and a single-piece GPU, paying special attention to the time proportion of the GBS and RT sections when processing different numbers of rays, as well as the acceleration factor of the GPU relative to the CPU. The GPU utilization is also analyzed using NVIDIA’s Nsight Compute tool.

4.5. Discussion of two major examples

In the simulation of this algorithm, atmospheric conditions including air temperature, relative humidity, and atmospheric pressure are assumed. These parameters are key factors affecting sound wave propagation, as they

Table 2: Free field case information with detailed descriptions

Parameter	Value
T_a : Air temperature ($^{\circ}\text{C}$)	20
H_r : Relative humidity (%)	70
P_a : Atmospheric pressure (atm)	1
f_s : Number of source frequencies	5
$\text{Im}(b)$: Imaginary component of beam parameter	-45874
N_b : Total number of buildings	1000
N_t : Total number of terrain grid points	4000
N_r : Total number of roads	5000
N_w : Number of water bodies (negative for exclusion)	-10
N_{tree} : Number of trees (negative for exclusion)	-10
D : Simulation dimensionality (3D or 2D)	3D
Θ_{min} : Minimum elevation angle	0
Θ_{max} : Maximum elevation angle	180
Φ_{min} : Minimum azimuthal angle	0
Φ_{max} : Maximum azimuthal angle	360
N_{steps} : Total time steps	8000
R_{max} : Maximum number of sound reflections allowed	10
Δt : Duration of a single time step (s)	0.0001
N_o : Total number of observation points	13586

directly influence the speed of sound and its interaction with the environment. The imaginary part of the single sound source frequency and beam parameters in the GBT data is an important component of the analysis, helping us construct a more realistic sound propagation model. Moreover, by setting different observation angles (Θ and Φ representing elevation and azimuth angles, respectively) and time steps (e.g., 5000 time steps, each step 0.0001 seconds), we are able to capture the propagation paths of sound waves at a higher resolution. The flow impedance setting for environmental elements is set to -10, indicating that all walls and obstacles are considered as hard surfaces, meaning that sound waves will reflect off them instead of penetrating. This setting is based on the characteristics of building materials commonly found in city environments. The observation points set in the model not only show the spatial distribution of sound wave propagation but also provide a comprehensive perspective for sound field analysis. The specific input information is illustrated in Tables 2 and 3.

Table 3: City case information with detailed descriptions

Parameter	Value
T_a : Air temperature ($^{\circ}\text{C}$)	20
H_r : Relative humidity (%)	70
P_a : Atmospheric pressure (atm)	1
f_s : Number of source frequencies	1
$\text{Im}(b)$: Imaginary component of beam parameter	-45874
N_b : Total number of buildings	-10
N_t : Total number of terrain grid points	-10
N_r : Total number of roads	-10
N_w : Number of water bodies (negative for exclusion)	-10
N_{tree} : Number of trees (negative for exclusion)	-10
D : Simulation dimensionality (3D or 2D)	3D
Θ_{min} : Minimum elevation angle	0
Θ_{max} : Maximum elevation angle	180
Φ_{min} : Minimum azimuthal angle	0
Φ_{max} : Maximum azimuthal angle	360
N_{steps} : Total time steps	5000
R_{max} : Maximum number of sound reflections allowed	20
Δt : Duration of a single time step (s)	0.0001
N_o : Total number of observation points	10201

In the "City environment" case, acoustic simulations are conducted for a complex city environment. As illustrated in Fig. 4.1, the model integrates a variety of environmental elements, including buildings, terrain, and roads. The combination of these elements not only reflects the diversity of city environments but also provides realistic simulation conditions for the propagation of sound waves through multiple obstacles. In contrast, the "Free Field" case study involves simulations in an open space environment without obstacles, hence it does not involve the setting of complex environmental elements. This distinction between the two environment allows for a comprehensive analysis of sound propagation behaviors in different settings, highlighting the effects of city structures on acoustic phenomena.

4.5.1. Numerical analysis of city environment

Our GPU multithreaded algorithm demonstrated significant acceleration compared to the traditional CPU single-threaded algorithm in the "city en-

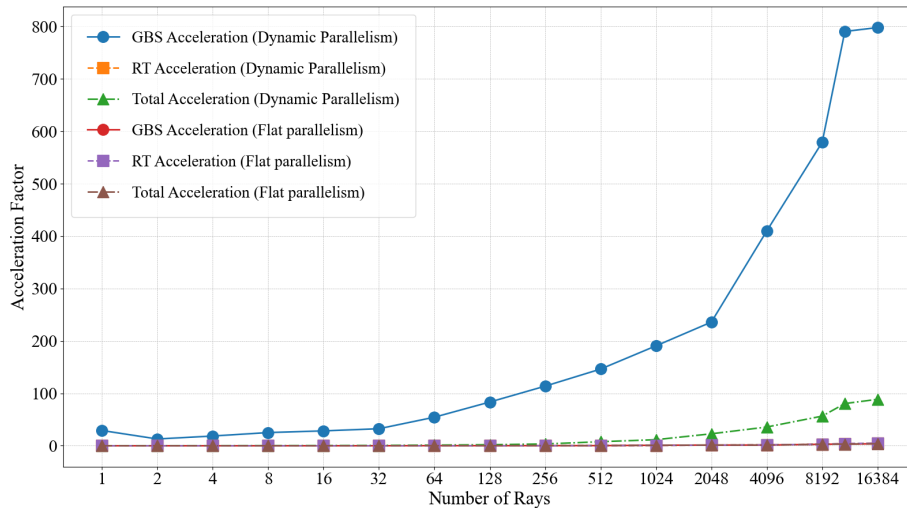


Figure 13: Performance of multithreaded GPU sound field prediction in city environments using dynamic parallelism: Acceleration factors for different ray counts.

viroment” experiment. This is particularly evident when the number of rays is increased to 16384, with the acceleration of the GBT reaching an impressive 798 times and the overall acceleration reaching approximately 88 times. These remarkable results are clearly illustrated in Figure. 13. The increased thread-parallel computing power provided by GPU dynamic parallelism is the main reason for the significant performance improvement. Furthermore, the timeshare analysis of the GBS and RT components clearly identifies a performance bottleneck in the sound field prediction algorithm. In multi-threaded GPU execution, the time taken by the GBS component is significantly reduced to the extent that RT occupies more than 90% of the time, as shown in Figure. 14. This highlights the significant advantage of GPU dynamic parallelism in processing complex acoustic computations. The overall acceleration ratio is nearly an order of magnitude greater than the acceleration ratio of the GBS component. The limitation of parallel acceleration potential is solely due to the serial execution of the RT part of the computation in a single thread. Nevertheless, the GPU multithreaded sound field prediction algorithm demonstrates significant acceleration, up to a hundred times in complex environments.

During the “City environment” experiment, it is observed that the GPU’s memory capacity limited the number of rays that could be processed simul-

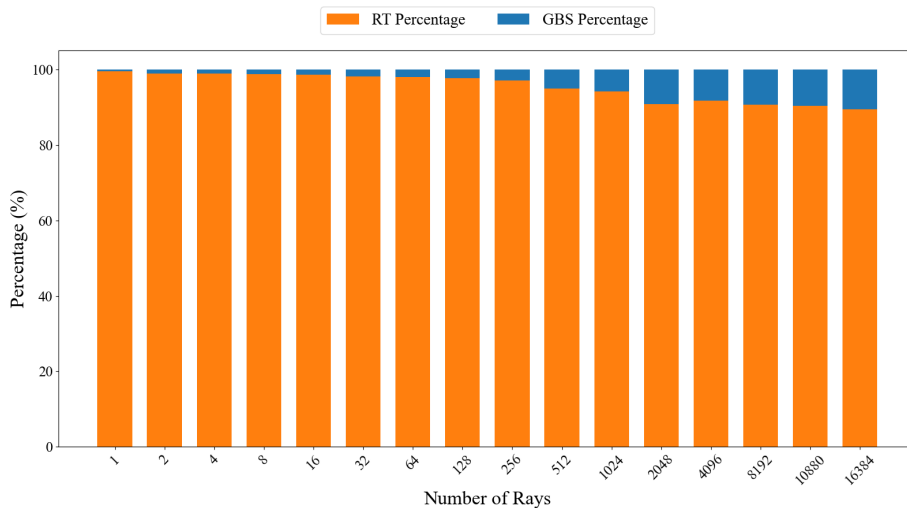


Figure 14: Percentage of two main processes in a multi-threaded sound field prediction algorithm in city environments using dynamic parallelism GPUs.

taneously. The maximum ray processing capacity is determined to be 11,364 rays, while the experiment involved 16,384 rays, exceeding this limit. To address this issue, a chunking mechanism is introduced, which involves dividing the large-scale ray computation task into multiple smaller chunks to accommodate the memory capacity constraints. This mechanism allows the GPU to effectively handle several rays that exceed its one-time maximum processing capability. Notably, after implementing the chunk processing operation, the acceleration factor for GBS reached 798 times, which is close to the 790 times acceleration factor observed with 10,800 rays previously. This result indicates that, despite the introduction of chunk processing adding additional overhead for memory management and computation scheduling, the acceleration factor remains at a high level and tends to converge with the increase in the number of processing chunks. This phenomenon reveals the stability and efficiency of the GPU multi-threaded algorithm in handling large-scale sound field prediction tasks.

4.5.2. Numerical analysis of free-field environment

The "Free Field" scenario exhibit particularly noteworthy performance when the number of rays increased to 16,384. Although the acceleration factor for GBS only reached 200 times, the overall acceleration factor sig-

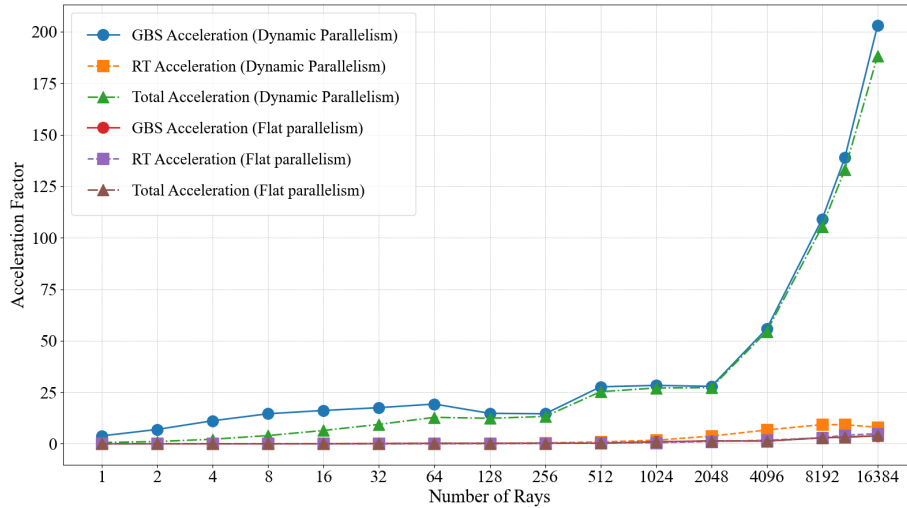


Figure 15: Performance of multithreaded GPU sound field prediction in free field environments using dynamic parallelism: Acceleration factors for different ray counts.

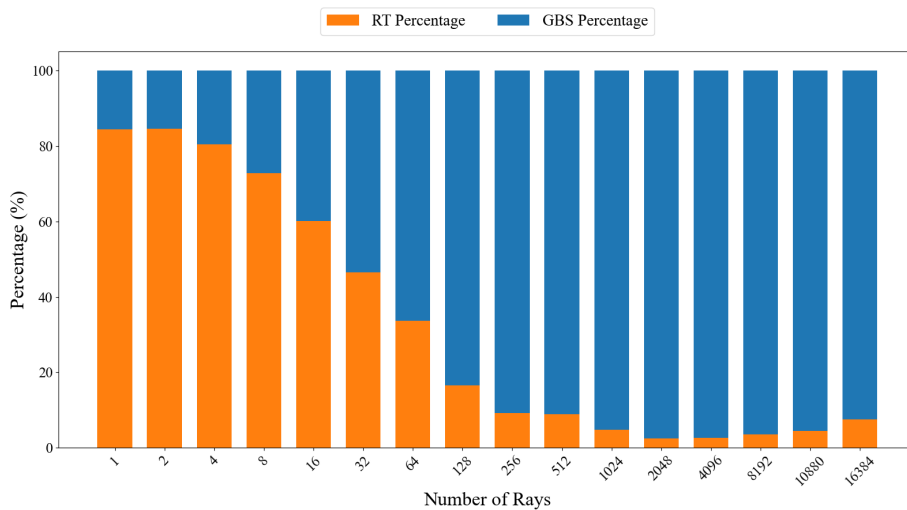


Figure 16: Percentage of two main processes in a multi-threaded sound field prediction algorithm in free field environments using dynamic parallelism GPUs.

nificantly rose to 188 times, as illustrated in Fig. 15. A shift in the time proportion between the RT module and the GBS module occurred, as shown in Fig. 16, where the roles reversed in terms of their contribution to the total computation time.

The unusual bar chart highlights the performance dynamics of the sound field prediction algorithm across different environment. Initially, the RT phase occupies a higher proportion of the computational load, while the GBS phase remains relatively low. This reason is that, with a smaller number of rays, the GBS phase has fewer Gaussian beams to sum, resulting in lower computational demand. However, as the number of rays increases, the workload for GBS escalates significantly due to the larger number of beams that need to be processed. In contrast, the RT phase experiences less pressure increase, especially in a free field scenario where there are no complex architectural elements to trace. This results in the chart showing a higher proportion of RT initially, followed by a dominant GBS proportion as the ray count grows. This pattern effectively illustrates the shifting computational burden between RT and GBS as the complexity of the ray interactions increases.

4.5.3. Analysis of GPU Utilisation Resource Levels

The analysis of GPU resource utilization is conducted using Nsight compute during the city scenario experiment. The results are presented in Tables 4, 5, and 6.

Table 4: Optimized Nsight compute software performance analysis table

Metric	Throughput [%]
Compute (SM) Throughput	22.27
Memory Throughput	9.16
L1/TEX Cache Throughput	13.15
L2 Cache Throughput	9.16
DRAM Throughput	2.04

A significant change observed in Table 4 is the substantial increase in the utilization of Streaming Multiprocessors (SM) resources from a mere 3.23% to 22.27% by implementing dynamic parallel processing for the GBS section. This significant improvement indicates that the dynamic parallelism strategy plays a key role in enhancing the efficiency of GPU computational resource utilization.

Table 5: Performance analysis of the Nsight compute software for Ray tracing process graph

Metric	Throughput [%]
Compute (SM) Throughput	1.67
Memory Throughput	3.05
L1/TEX Cache Throughput	4.38
L2 Cache Throughput	3.05
DRAM Throughput	0.32

As seen in Table 5, the complexity of the computation leads to a higher demand for registers per GPU thread, with an average of 199 registers needed. This high register demand poses a limitation on the granularity of dynamic parallelism. Registers are a highly valuable resource in GPUs, and the excessive consumption of registers by each thread means that fewer threads can be executed simultaneously. Therefore, our dynamic parallelism optimization strategy is approaching its performance limit under the current conditions.

Table 6 shows that the GPU utilization rate for executing the RT module alone is only 1.67%, a low utilization rate that significantly drags down the overall GPU performance. This indicates significant room for performance improvement during the RT process. Thus, a focus of future work could be to further optimize the RT algorithm to improve its resource utilization efficiency on the GPU, thereby achieving a higher acceleration ratio and better performance for the overall sound field prediction algorithm.

Table 6: Analysis of the resources used by the optimised

Launch Statistics	Value
Grid Size	6
Registers Per Thread	199
Block Size	256
Thread	1536
Waves Per SM	0.13

5. Conclusion

This study successfully reconstructed the Gaussian Beam Tracing (GBT) method using CUDA, enabling efficient GPU acceleration for complex acous-

tic simulations. By leveraging both flat and dynamic parallelism, the proposed method addresses computational challenges such as irregular loops and GPU memory limitations, significantly improving performance and scalability. The key findings and contributions of this work are as follows:

Substantial performance gains: The GPU-accelerated GBT algorithm demonstrated significant acceleration, achieving up to 790 times speedup in city environments and 188 times speedup in free-field environments compared to the original CPU-based implementation. These results establish the effectiveness of the proposed method in handling large-scale acoustic simulations in diverse scenarios.

Innovative algorithmic enhancements: This study introduced a dynamic parallelism approach to efficiently process the non-uniform computational load of Gaussian beam summation (GBS). By enabling threads to launch new threads dynamically, the method effectively balanced workloads, minimized idle resources, and overcame the limitations of flat parallelism in scenarios with highly variable computational demands.

Comprehensive evaluation: Extensive numerical experiments validated the accuracy of the GBT method against analytical solutions and assessed its performance in both free-field and city environments. The proposed chunking mechanism for managing GPU memory further ensured scalability for processing a large number of rays.

Scalability and practical applications: The findings highlight the potential for real-time sound field prediction in applications such as architectural acoustics, environmental noise analysis, and virtual reality. The integration of GPU-accelerated algorithms offers a robust foundation for future developments in high-performance acoustic simulations.

Acknowledgments

This work was supported in part by the National Natural Science Foundation of China (No. 12302346) and Zhejiang Provincial Natural Science Foundation of China (No. LQ24A040014).

References

- [1] John C Allred and Albert Newhouse. Applications of the Monte Carlo method to architectural acoustics. *The Journal of the Acoustical Society of America*, 30(1):1–3, 1958.

- [2] Michael Barron. *Auditorium Acoustics and Architectural Design*. Spon Press, 2009.
- [3] Michael Vorländer. Virtual acoustics. *Archives of Acoustics*, 39(3):307–318, 2014.
- [4] Nikunj Raghuvanshi, Rahul Narain, and Ming C Lin. Efficient and accurate sound propagation using adaptive rectangular decomposition. *IEEE Transactions on Visualization and Computer Graphics*, 15(5):789–801, 2009.
- [5] Qichen Tan, Haoyu Bian, Jingwen Guo, Peng Zhou, Hong Kam Lo, Siyang Zhong, and Xin Zhang. Virtual flight simulation of delivery drone noise in the urban residential community. *Transportation Research Part D: Transport and Environment*, 118:103686, 2023.
- [6] Haoyu Bian, Qichen Tan, Siyang Zhong, and Xin Zhang. Efficient computation of broadband noise propagation using Gaussian beam tracing method. *The Journal of the Acoustical Society of America*, 151(5):3387–3397, 2022.
- [7] Qichen Tan, Yuhong Li, Han Wu, Peng Zhou, Hong Kam Lo, Siyang Zhong, and Xin Zhang. Enhancing sustainable urban air transportation: Low-noise UAS flight planning using noise assessment simulator. *Aerospace Science and Technology*, 147:109071, 2024.
- [8] Qichen Tan, Siyang Zhong, Renhao Qu, Yuhong Li, Peng Zhou, Hong Kam Lo, and Xin Zhang. Low-noise flight path planning of drones based on a virtual flight noise simulator: A vehicle routing problem. *IEEE Intelligent Transportation Systems Magazine*, 2024.
- [9] JA Eaton and BA Regan. Application of the finite element method to acoustic scattering problems. *AIAA Journal*, 34(1):29–34, 1996.
- [10] Carl R Hart and Siu-Kit Lau. Prediction of urban sound propagation via adaptive beam tracing. *The Journal of the Acoustical Society of America*, 129(4):2481–2481, 2011.
- [11] Eduard Deines, Martin Bertram, Jan Mohring, Jevgenij Jegorovs, Frank Michel, Hans Hagen, and Gregory M Nielson. Comparative visualization for wave-based and geometric acoustics. *IEEE Transactions on Visualization and Computer Graphics*, 12(5):1173–1180, 2006.

- [12] Hanbo Jiang, Xin Zhang, and Xun Huang. Reduced-basis boundary element method for efficient broadband acoustic simulation. *Journal of Sound and Vibration*, 456:374–385, 2019.
- [13] Samuli Laine, Samuel Siltanen, Tapio Lokki, and Lauri Savioja. Accelerated beam tracing algorithm. *Applied Acoustics*, 70(1):172–181, 2009.
- [14] Jont B Allen and David A Berkley. Image method for efficiently simulating small-room acoustics. *The Journal of the Acoustical Society of America*, 65(4):943–950, 1979.
- [15] Hilmar Lehnert. Systematic errors of the ray-tracing algorithm. *Applied Acoustics*, 38(2-4):207–221, 1993.
- [16] Asbjørn Krokstad, Staffan Strom, and Svein Sørsdal. Calculating the acoustical room response by the use of a ray tracing technique. *Journal of Sound and Vibration*, 8(1):118–125, 1968.
- [17] Michael B Porter and Homer P Bucker. Gaussian beam tracing for computing ocean acoustic fields. *The Journal of the Acoustical Society of America*, 82(4):1349–1359, 1987.
- [18] Michael B Porter and Yong-Chun Liu. Finite-element ray tracing. *Theoretical and computational acoustics*, 2:947–956, 1994.
- [19] Bingsheng He, Mian Lu, Ke Yang, Rui Fang, Naga K Govindaraju, Qiong Luo, and Pedro V Sander. Relational query coprocessing on graphics processors. *ACM Transactions on Database Systems (TODS)*, 34(4):1–39, 2009.
- [20] Cristobal A Navarro, Nancy Hitschfeld-Kahler, and Luis Mateu. A survey on parallel computing and its applications in data-parallel problems using GPU architectures. *Communications in Computational Physics*, 15(2):285–329, 2014.
- [21] Josef Spjut, Andrew Kensler, Daniel Kopta, and Erik Brunvand. TRaX: A multicore hardware architecture for real-time ray tracing. *IEEE Transactions on Computer-Aided Design of Integrated Circuits and Systems*, 28(12):1802–1815, 2009.

- [22] Brent Cowan and Bill Kapralos. GPU-based real-time acoustical occlusion modeling. *Virtual Reality*, 14:183–196, 2010.
- [23] Konstantinos Gkanos, Finnur Pind, Hans Henrik Brandenborg Sørensen, and Cheol-Ho Jeong. Comparison of parallel implementation strategies for the image source method for real-time virtual acoustics. *Applied Acoustics*, 178:108000, 2021.
- [24] Jundong Tan, Zhuo Su, and Yunliang Long. A full 3-D GPU-based beam-tracing method for complex indoor environments propagation modeling. *IEEE Transactions on Antennas and Propagation*, 63(6):2705–2718, 2015.
- [25] M De Greef, J Crezee, JC Van Eijk, R Pool, and Arjan Bel. Accelerated ray tracing for radiotherapy dose calculations on a GPU. *Medical Physics*, 36(9Part1):4095–4102, 2009.
- [26] Design Guide. CUDA C programming guide. *NVIDIA*, July, 29:31, 2013.
- [27] Ben Cope, Peter YK Cheung, Wayne Luk, and Lee Howes. Performance comparison of graphics processors to reconfigurable logic: A case study. *IEEE Transactions on Computers*, 59(4):433–448, 2010.
- [28] Pawel Czarnul. Programming, tuning and automatic parallelization of irregular divide-and-conquer applications in DAMPVM/DAC. *The International Journal of High Performance Computing Applications*, 17(1):77–93, 2003.
- [29] L. Speer and Xiaohang Yue. An updated cross-indexed guide to the ray-tracing literature. *Computers & Graphics*, 1992.